Beam Physics Note
TRI-BN-23-22
November 27, 2023

Primary Achromaticity of the HEBT2 and HEBT3 Beamlines

Olivier Shelbaya, Alexander Katrusiak

TRIUMF

Abstract: An investigation of the HEBT bend modules, consisting of two 22.5° dipole magnets coupled with short magnetic quadrupoles, reveals chromatic couplings induced in the beam distribution. This report presents this finding in the design tune.

1 Background

In the report TRI-DN-99-23[1], the design specification for the HEBT2 and HEBT3 bend sections are presented (Fig. 1). The HEBT lines have been implemented in `TRANSOPTR`, detailed in [2].

This report presents a brief analysis of the HEBT bend section tune and optics. We show that the standard bend modules used in HEBT2 and HEBT3 are in fact chromatic, resulting in nonzero couplings between dimensions (1,2) and (5,6), the horizontal and longitudinal bunch coordinates.

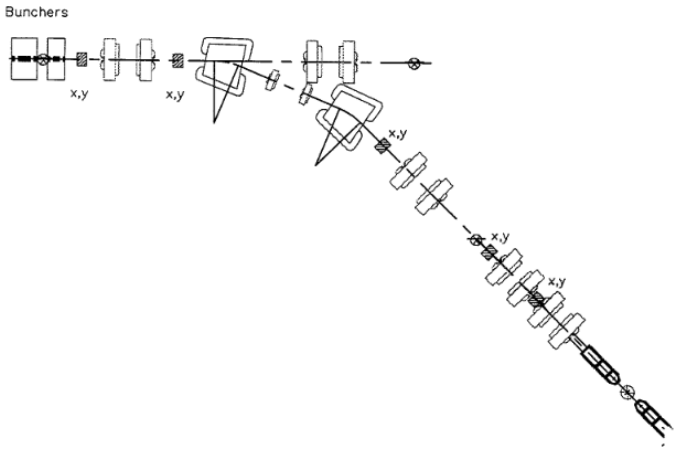

Figure 1: Overview image of the HEBT2 dipole bending section, transporting beam from DTL to DRAGON experiment, taken from [1]. Beam propagates from top left to bottom right.

2 Chromatic Couplings and Dispersion

In the literature, dispersive couplings are often introduced using an inhomogeneous term to the solution to the Hill differential equation:

$$\frac{\mathrm{d}^2 x(s)}{\mathrm{d}s^2} + k(s)x(s) = \frac{1}{\rho(s)}\frac{\Delta P(s)}{P_0} \tag{1}$$

producing the solution for the x-coordinate:

$$x(s) = x_0 + D(s)\frac{\Delta P(s)}{P_0} \tag{2}$$

with the dispersion function $D(s)$ defined as the solution to the equation:

$$D''(s) + k(s)D(s) = \frac{1}{\rho(s)}. \tag{3}$$

The solution $D(s)$ records the expected transverse displacement of a particle per percent momentum deviation. Dispersive bending elements such as magnetic dipoles will change the dispersion and its derivative. Quadrupoles, since they are non-dispersive (ρ^{-1}=0) will not initiate chromaticity in a beam, but will alter it if nonzero. The beam distribution at any given location s=s_1 is said to be *singly* achromatic when $D(s_1) = 0$ but $D'(s_1) \neq 0$. Likewise, double achromaticity in a section implies $D(s_1) = D'(s_1) = 0$. In the former case, there will be chromatic couplings at locations other than s_1, while in the latter, the tune is achromatic everywhere downstream of the final dipole bender. In terms of the beam or sigma matrix formalism, chromaticity is manifest when there are couplings between dimensions (1,2) and (5,6), assuming a state vector $\mathbf{X} = (x, x', y, y', z, z')$. For an *a priori* uncoupled beam matrix amongst canonical coordinate pairs, chromatic couplings are evidenced by nonzero transfer matrix elements M_{16}, linking (x, z').

3 Bend Chromaticity

The dipole bends in HEBT2 and HEBT3 have been taken from [2] and the quadrupole gradients have been set to that which is listed in Table 8, p.16 under the heading *achromatic bend mode*. This is shown in Figure 2. The transfer matrix element M_{16} is plotted as the orange trace on the figure. The design tune produces near zero dispersion at exit, though the derivative $D'(s)$ is nonzero, evidenced by the behaviour of M_{16}. This means locations downstream of the HEBT2/HEBT3 bends are not doubly achromatic.

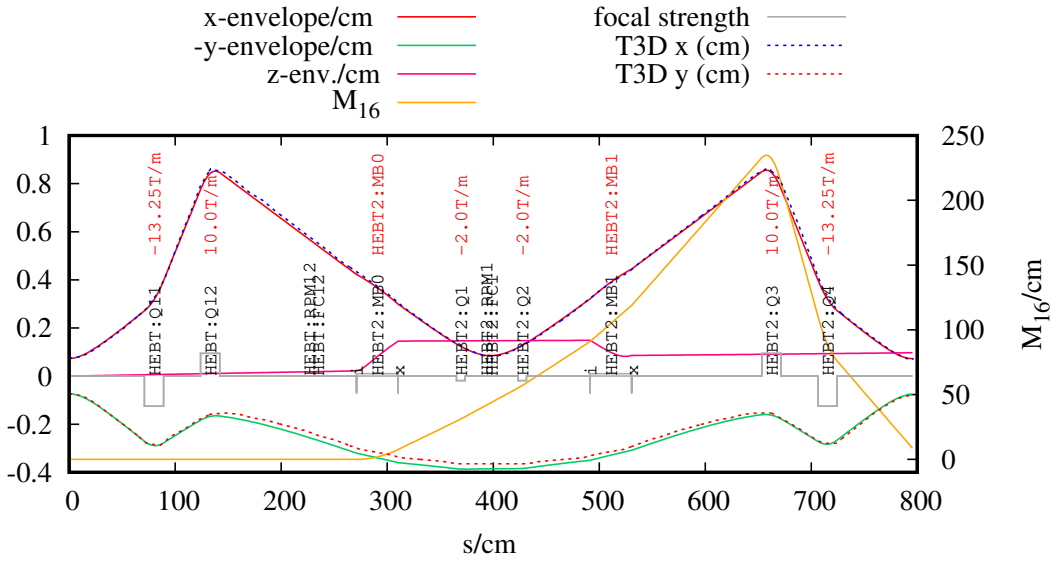

Figure 2: TRANSOPTR simulation of the HEBT 45° bend section, using the achromatic design tune from Table 8, p.16 in [1]. Original T3D simulation envelopes recorded in [2] are shown as dotted lines on the plot. An A/q=6, E/A=1.5MeV/u beam is shown.

Finding 1: The design tune of the 45° HEBT2/3 bend sections is chromatic.

For completeness, the *dispersed focus mode* tune is shown in Figure 3.

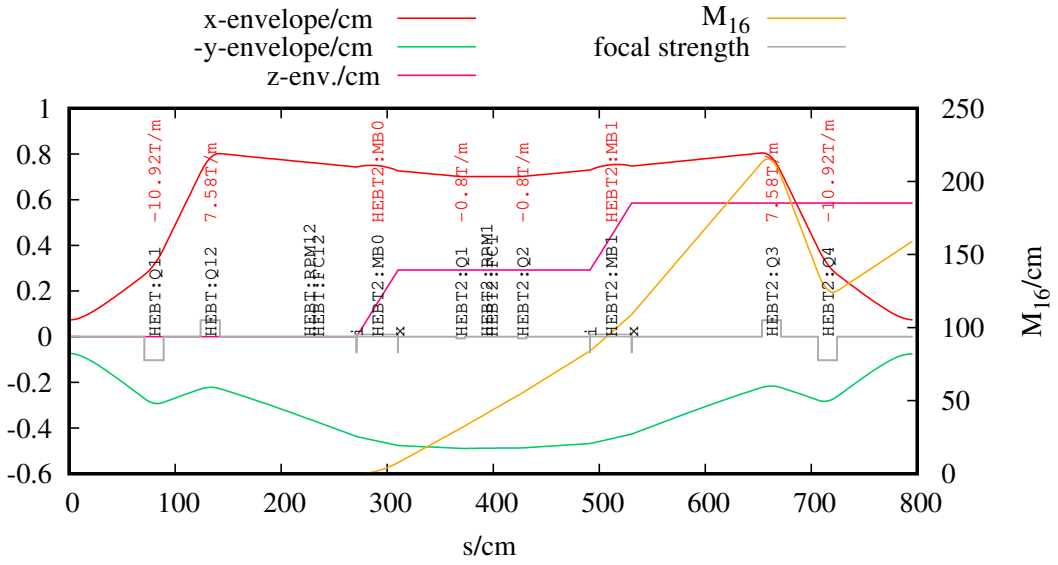

Figure 3: TRANSOPTR simulation of the HEBT 45° bend section, using the dispersed focus design tune from Table 9, p.17 in [1]. An A/q=6, E/A=1.5MeV/u beam is shown.

4 HEBT2 Corner Envelope Simulations

In Figure 4, the short quadrupoles HEBT2:Q1 and Q2 (HEBT3:Q1/Q2) [3] are operated at a sufficient gradient to cause double achromaticity in the bend. This requires reversing their polarity and operating them at nearly 9 times higher field gradient, when compared to the tunes presented in [1]. In the report TRI-DNA-99-05[3], the maximum gradient for the short quadrupoles is specified at 3T/m. This means that, for an A/q=6 beam at E/A=1.5MeV/u, the quadrupoles are underpowered by a factor of more than five. This will vary depending on the mass to charge ratio.

Finding 2: The HEBT2/3 'trim' quadrupoles used in the 45° bend sections are of incorrect polarity and insufficiently powerful to cause double achromaticity in the tune to DRAGON.

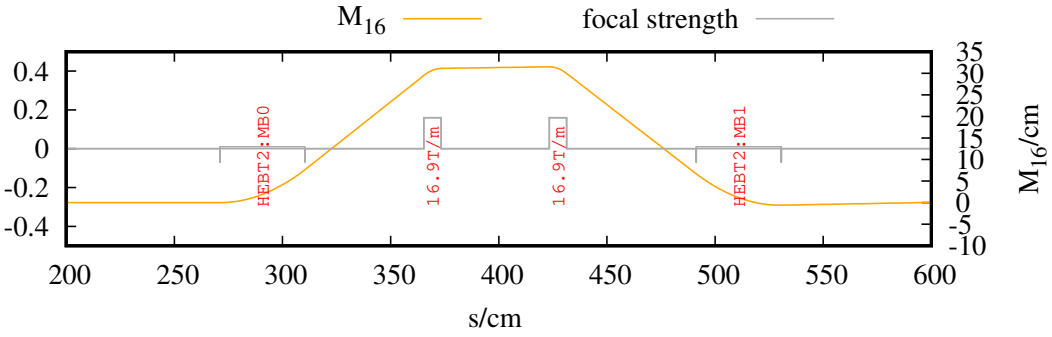

Figure 4: TRANSOPTR simulation of the HEBT 45° bend section, where the short inter-dipole quadrupoles HEBT2:Q1 and HEBT2:Q2 (or HEBT3:Q1, HEBT3:Q2) are operated at a sufficient gradient to cause double achromaticity. This requires a gradient almost 9 times higher than in [1]. An A/q=6, E/A=1.5MeV/u beam is shown.

5 Discussion

5.1 DRAGON Gas Chamber Transmission

The short quadrupoles located between HEBT2 and HEBT3 dipoles are of the wrong polarity and possess insufficient strength to remove chromatic couplings in the beam from DTL. Together with the findings in [4] on the MEBT corner, this suggests that beams sent to the HEBT stations are consistently chromatic. The computed DRAGON gas chamber transmission versus longitudinal divergence is shown in Figure 5, showing the consequences of aperture losses along the horizontal axis. This is further illustrated in Fig. 6 shows the consequences of operating HEBT2 line without energy spread minimization: There is a coupling between the beam's energy spread and the horizontal waist in the DRAGON gas chamber.

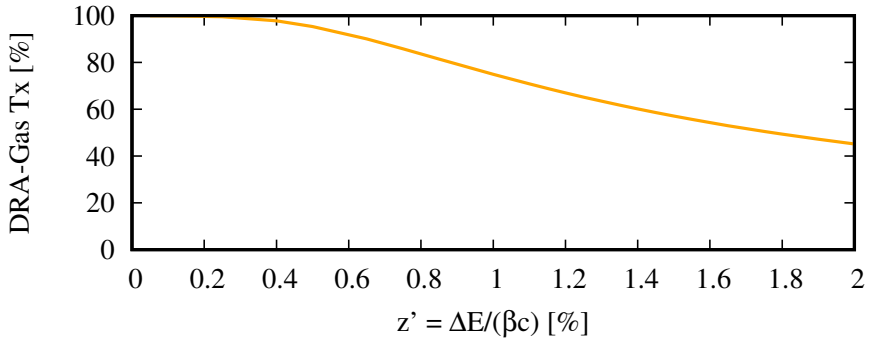

Figure 5: TRANSOPTR computed DRAGON gas chamber transmission, assuming a 4 mm half-aperture in (x,y).

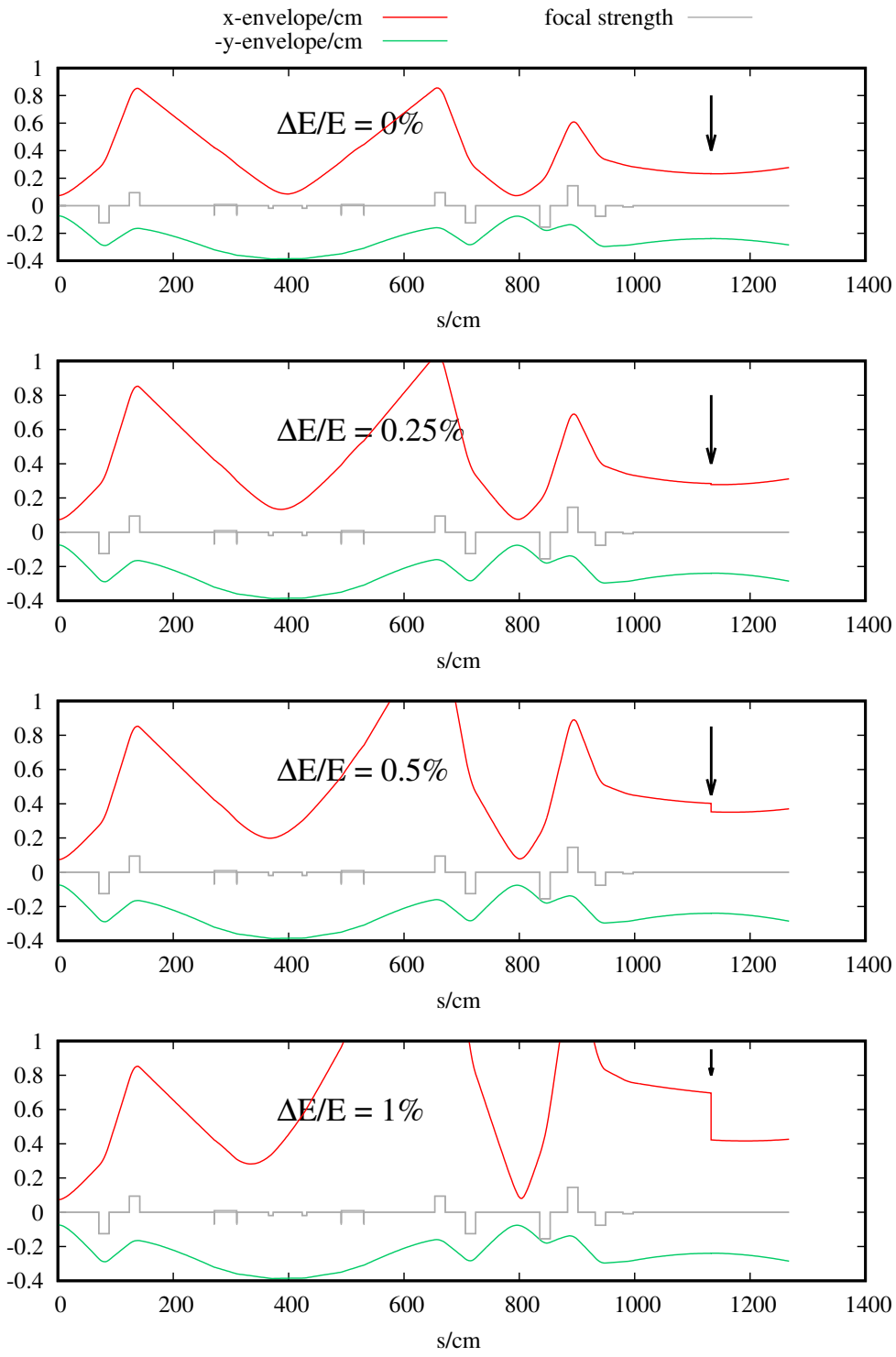

Figure 6: `TRANSOPTR` simulations from object point of HEBT2 module, up to DRAGON gas chamber focus, showcasing final spot size dependence upon beam energy spread. A 1 cm z-envelope size has been used in each case. Subroutine `slit`[5] has been used for aperture loss simulation. Vertical arrow indicates DRAGON gas chamber location, with simulated half-width aperture of 4 mm in (x,y).

5.2 Dispersion Suppression at DRAGON

Since the dispersive coupling inherited in the HEBT2 (or HEBT3) bend sections induces correlations between (x, x') and (z, z'), a straightforward way to minimize such couplings is to reduce the beam's longitudinal divergence (z'=$\Delta E/(\beta c)$) by establishing an energy focus at DRAGON (or at HEBT3).

Figure 7 shows longitudinal envelopes starting at the HEBT 11 and 35 MHz bunchers and terminating at the DRAGON gas chamber. The 35 MHz buncher has been used[1] to minimize z' (debunching; energy focus). On the plot, dotted lines correspond to bunchers off operation, where a large M_{16} can be seen on the right hand vertical axis: This is the chromatic coupling inherited by the corner.

By reducing the energy spread (Fig. 7, solid lines), the magnitude of M_{16} is greatly diminished, effectively suppressing the beam's chromaticity. As discussed in the previous section, this in turn will reduce potential broadening of the horizontal beamspot inside DRAGON's gas chamber.

[1] See Fig. 14 in [1] to see E/A ranges for 11MHz and 35MHz HEBT bunchers.

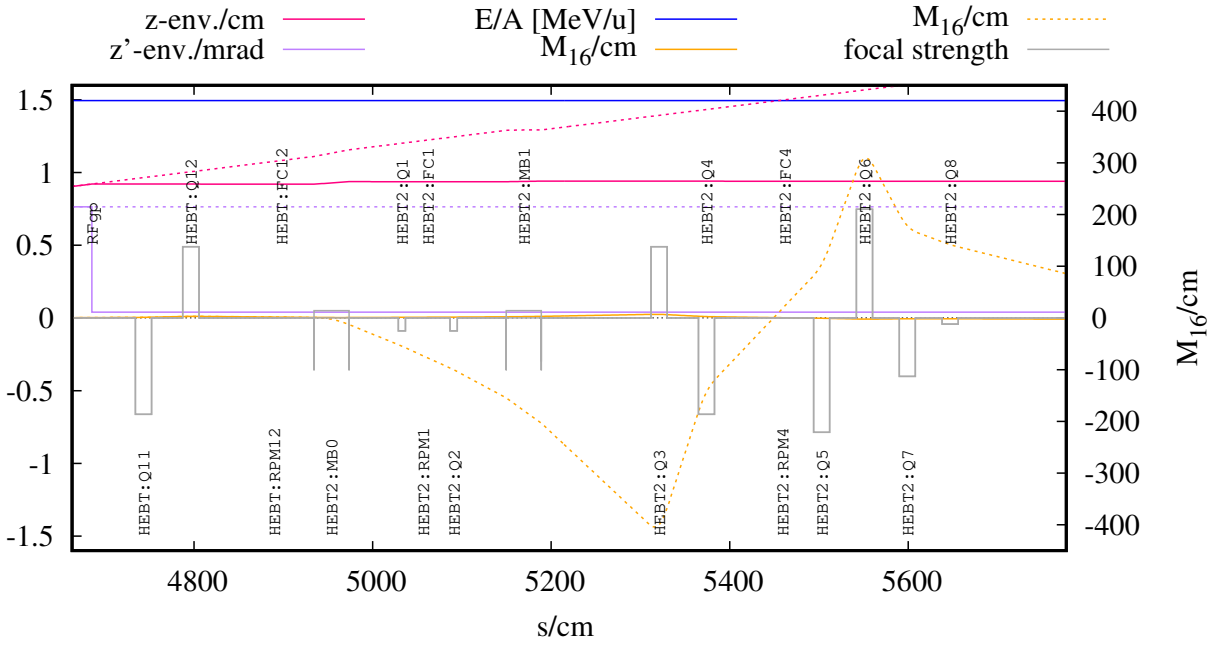

Figure 7: TRANSOPTR simulations from RFQ exit at start of MEBT section, up to DRAGON gas chamber focus, showcasing final spot size dependence upon beam energy spread. MEBT bunch rotator set for beam debunching shown, without a stripping foil. This significantly reduces chromatic couplings throughout the linac, up to the HEBT2 45° bend.

6 HEBT Machine Development Report

The DTL Autofocus model reported in [6] was used to tune the DTL and HEBT-HEBT2 lines for a $^{12}C^{3+}$ beam at E/A=1.53 MeV/u during a machine development shift. Beam was injected into DTL per standard procedure at E/A=0.153 MeV/u. Rotary profile monitor (RPM) scans of the beam intensity distribution were recorded in the HEBT and HEBT2 lines, after manual threading using magnetic steerers. The fit envelopes are shown at the top of Figure 8.

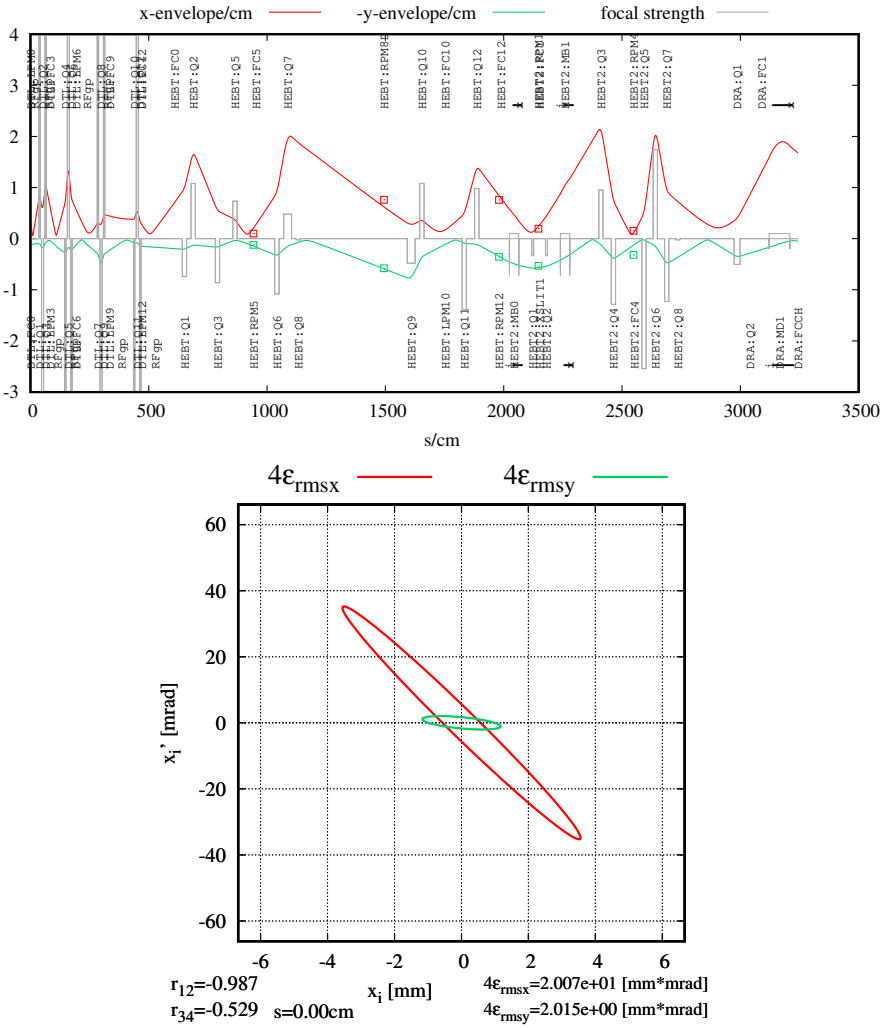

Figure 8: **Top:** `TRANSOPTR` envelope fit performed on-line with a $^{12}C^{3+}$ beam at E/A=0.720 MeV/u. Profile monitor 2rms sizes are shown as squares on the plot. **Bottom:** Fit beam distribution at DTL injection.

For this fit, the on-line 2rms sizes were extracted with the `profiles` package[7], and these were fed to the on-line model using `twissify`'s RPM fitting routine. `TRANSOPTR` then performed a 6-parameter fit for twiss parameters $(\alpha_x, \beta_x, \epsilon_x, \alpha_y, \beta_y, \epsilon_y)$ using the RPM sizes as fit constraints using `fitsz`. The DTL model uses subroutine `rfgap`, causing (unphysical) stepwise energy increase inside the IH resonators, while transversely they equivalent to a drift in free space.

The injected DTL beam distributions, from this fit, for horizontal and vertical dimensions are shown at the bottom of Figure 8. Observe the order-of-magnitude size difference between beams in the x (horizontal; dispersive) and y (vertical; non dispersive) planes. Based on a past tomographic investigation of RFQ output beams [8], which found beams of roughly the same emittance in (x, y) at the modulated rf quadrupole's output, the fit presented in this report supports the findings in [4], in which a mix of quadrupole aberrations and transverse-longitudinal couplings cause emittance growth and a mismatch at DTL injection.

Figure 9 shows the DTL portion of the on-line fit. The correlation coefficient r_{12} spends a considerable amount of linac transit being at values near ± 1, due to the high eccentricity of the position-momentum distribution. This will cause further mismatch sensitivities in the HEBT lines, though it is also abated by the higher rigidity of the beam which requires the quadrupole lenses be operated at higher gradients, where residual magnetization errors are proportionally lesser.

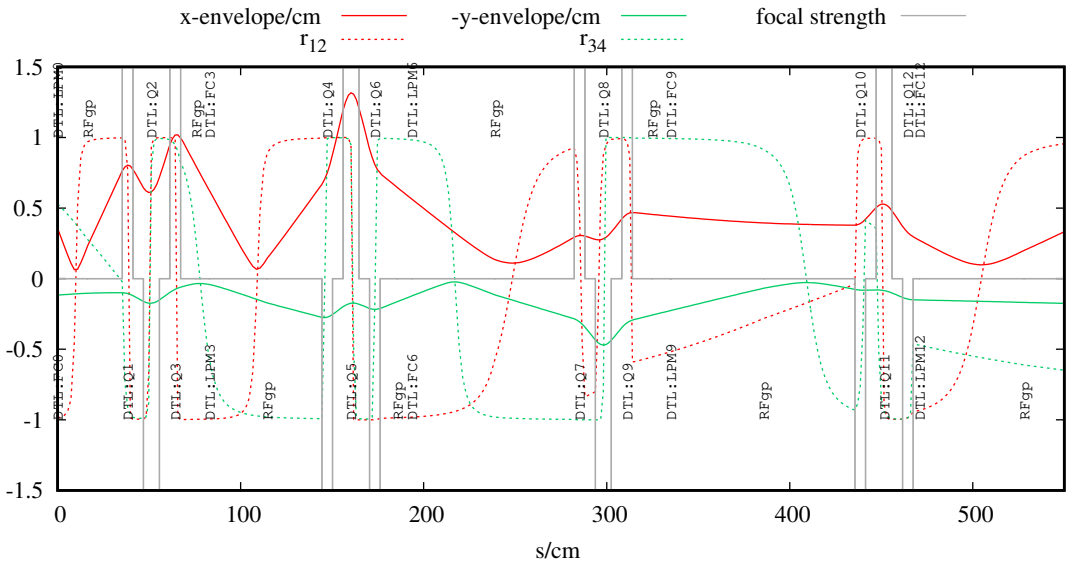

Figure 9: From the fit in Figure 8, this is a detail view of the fit beam envelopes through the on-line DTL tune, including correlation coefficients for both transverse distributions.

6.1 Inferred DRAGON Gas-Target Beamspot

The beam-based fit that has been presented in Figure 8 further enables extraction of the 4rms containment ellipses at the location of DRAGON's gas chamber, enabling predictive on-line monitoring of the spot at experiment by way of the HEBT/HEBT2 line RPMs and the on-line model.

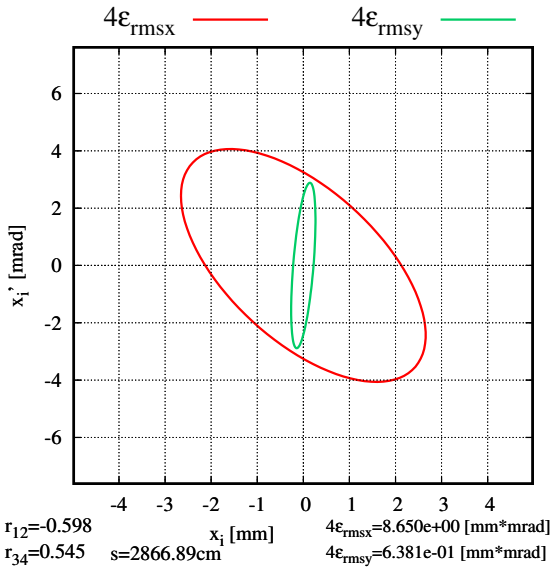

Figure 10: 4rms beam containment ellipses for the x (horizontal) and y (vertical) dimensions, at the location of DRAGON's gas target. Distributions are based on the model fit shown in Figure 8.

7 Conclusion

This report has outlined recent analysis and modelling of the HEBT beamlines. We have identified a key optical issue in the beamline: Chromatic couplings are induced by the HEBT2 and HEBT3 bends. At the DRAGON experiment, this causes a relationship between the longitudinal beam divergence and hence energy spread (z'=$\Delta E/(\beta c)$ which was shown to cause broadening of the horizontal beamsize at the DRAGON gas target. The short HEBT2 quadrupoles are found to be too weak to zero both dispersion and its s-derivative downstream of the second dipole magnet in the bend. This insight will help define future operating procedures for DRAGON.

Beam-based modelling and fits were presented, supporting the hypothesis of emittance broadening and mismatch out of the MEBT section. We have shown that an on-line model of DTL, HEBT and HEBT2 can be used, together with HEBT RPM readings, producing transverse distributions at DTL entrance and at DRAGON's gas target.

References

[1] Robert Laxdal. Design Specification for ISAC HEBT. Technical Report TRI-DN-99-23, TRIUMF, 1999. http://lin12.triumf.ca/design-notes/1999/TRI-DN-99-23.PDF.

[2] Olivier Shelbaya. TRANSOPTR Implementation of the HEBT Beamlines. Technical Report TRI-BN-19-06, TRIUMF, 2019. http://beamphys.triumf.ca/~oshelb/physnotes/optrHEBT/optrHEBT.pdf.

[3] GM Stinson. A design for trim quadrupoles for the HEBT of ISAC. Technical Report TRI-DNA-99-05, TRIUMF, 1999. http://lin12.triumf.ca/design-notes/1999/TRI-DNA-99-05.PDF.

[4] Olivier Shelbaya. Beam Dynamics Study of ISAC-MEBT. Technical Report TRI-BN-22-29, TRIUMF, 2022. https://beamphys.triumf.ca/~oshelb/physnotes/optrMEBT2/optrMEBT2.pdf.

[5] Richard Baartman. SLIT routine for TRANSOPTR. Technical Report TRI-BN-19-21, TRIUMF, 2019. http://lin12.triumf.ca/text/design_notes/b2019_21/note.pdf.

[6] Olivier Shelbaya. On-Line Validation of DTL Autofocus. Technical Report TRI-BN-22-31, TRIUMF, 2022. https://beamphys.triumf.ca/~oshelb/physnotes/autofocus/autofocus.pdf.

[7] Kristin Wu. Profile Monitor Classification using Random Forest Classifier . Technical Report TRI-BN-21-11, TRIUMF, 2021. https://lin12.triumf.ca/text/design_notes/Kristin_Wu_Winter_2021/main.pdf.

[8] Olivier Shelbaya. Maximum Entropy Tomography at the ISAC-RFQ. Technical Report TRI-BN-20-12, TRIUMF, 2020. https://beamphys.triumf.ca/~oshelb/physnotes/optrTomo/optrTomo.pdf.